Analysis of Cholera Toxin−Ganglioside Interactions by Flow Cytometry†

Sabine Lauer,*,‡ Byron Goldstein,§ Rhiannon L. Nolan,‡ and John P. Nolan*,‡

Bioscience and Theoretical Divisions, Los Alamos National Laboratory, Los Alamos, New Mexico 87545

Received June 19, 2001

ABSTRACT: Cholera toxin entry into mammalian cells is mediated by binding of the pentameric B subunit (CTB) to ganglioside GM_1 in the cell membrane. We used flow cytometry to quantitatively measure in real time the interactions of fluorescently labeled pentameric cholera toxin B-subunit (FITC-CTB) with its ganglioside receptor on microsphere-supported phospholipid membranes. A model that describes the multiple steps of this mode of recognition was developed to guide our flow cytometric experiments and extract relevant equilibrium and kinetic rate constants. In contrast to previous studies, our approach takes into account receptor cross-linking, an important feature for multivalent interactions. From equilibrium measurements, we determined an equilibrium binding constant for a single subunit of FITC-CTB binding monovalently to GM_1 presented in bilayers of $\sim 8 \times 10^7$ M^{-1} while that for binding to soluble GM_1-pentasaccharide was found to be $\sim 4 \times 10^6$ M^{-1}. From kinetic measurements, we determined the rate constant for dissociation of a single site of FITC-CTB from microsphere-supported bilayers to be $(3.21 \pm 0.03) \times 10^{-3}$ s^{-1}, and the rate of association of a site on FITC-CTB in solution to a GM_1 in the bilayer to be $(2.8 \pm 0.4) \times 10^4$ M^{-1} s^{-1}. These values yield a lower estimate for the equilibrium binding constant of $\sim 1 \times 10^7$ M^{-1}. We determined the equilibrium surface cross-linking constant [$(1.1 \pm 0.1) \times 10^{-12}$ cm^2] and from this value and the value for the rate constant for dissociation derived a value of $\sim 3.5 \times 10^{-15}$ cm^2 s^{-1} for the forward rate constant for cross-linking. We also compared the interaction of the receptor binding B-subunit with that of the whole toxin (A- and B-subunits). Our results show that the whole toxin binds with ~100-fold higher avidity than the pentameric B-subunit alone which is most likely due to the additional interaction of the A_2-subunit with the membrane surface. Interaction of cholera toxin B-subunit and whole cholera toxin with gangliosides other than GM_1 revealed specific binding only to $GD1_b$ and asialo-GM_1. These interactions, however, are marked by low avidity and require high receptor concentrations to be observed.

Many biological toxins enter cells by a mechanism that begins with binding to specific receptors on a cell surface. The soluble ligands that interact with cell surface receptors may be monovalent as are some small peptide ligands, bivalent as are many large peptide hormones or antibodies, or of even higher valencies. The latter includes interactions between many microbial or plant toxins and cell surface gangliosides. Cholera toxin (CT)[1] entry into intestinal epithelial cells is mediated by binding of the pentameric B-subunit (CTB) to the ganglioside GM_1 in the cell's membrane. Notable features of this interaction include a low-affinity monovalent interaction between individual B-subunits and the carbohydrate moiety of GM_1, an effective high-affinity multivalent interaction between the pentameric B-subunit and several membrane-bound GM_1 molecules, and the lateral mobility of the GM_1 molecule within the bilayer membrane.

Thermodynamic and kinetic properties of the interaction of cholera toxin or its B-subunit with GM_1 have previously been investigated using traditional receptor binding methods, e.g., radioligands (*2*, *3*), and calorimetry (*4*), and more recently homogeneous methods, specifically surface plasma resonance [SPR; (*5*−*8*)]. While these SPR studies provided improved kinetic resolution, they used a single-site binding model to describe the toxin receptor interaction to interpret data generated mostly at a single receptor density. Since the interaction between cholera toxin and its cell surface receptor is multivalent, a complete description requires consideration of receptor cross-linking, a process that depends on receptor density and mobility.

In the present work, we have taken advantage of flow cytometry's ability to make sensitive and quantitative measurements of molecular interactions with continuous, subsecond kinetic resolution (*9*, *10*) to characterize in detail the multivalent interaction of CT with GM_1. We have developed a multistep model (see Figure 1) to guide our flow cytometric measurements and to extract equilibrium binding and kinetic rate constants. This is the first detailed mecha-

† This study was supported by NIH Grant RR01315 and LANL-LDRD Grant XATX.

* Address correspondence to these authors at the Bioscience Division, Los Alamos National Laboratory, MS 888, Los Alamos, NM 87545. E-mail: nolan@telomere.lanl.gov.

‡ Bioscience Division, Los Alamos National Laboratory.

§ Theoretical Division, Los Alamos National Laboratory.

[1] Abbreviations: CT, cholera toxin; CTB, cholera toxin B-subunit; SPR, surface plasmon resonance; FITC-CTB, fluorescein isothiocyanate-labeled CTB; FAM-CT, 6-carboxyfluorescein-labeled CT; MESF, mean equivalent of soluble fluorescein; Var, variance; eq(s), equation(s).

10.1021/bi0112816
Published on Web 01/17/2002

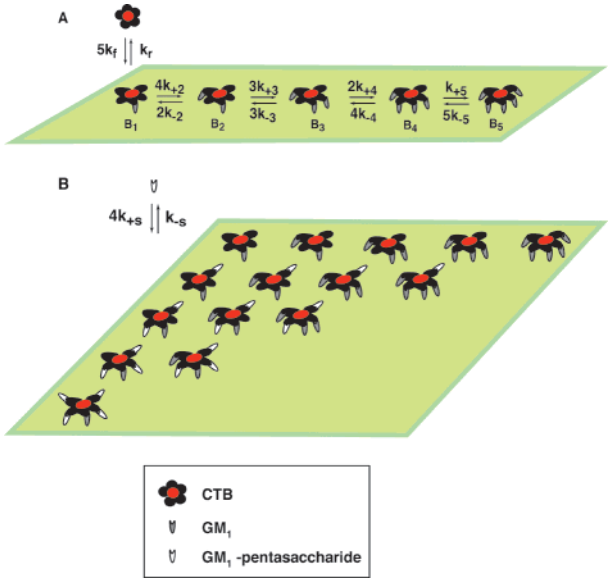

FIGURE 1: Model of the interactions of CTB with mobile GM_1-receptor confined to a spherical surface and competition of soluble GM_1-pentasaccharide with surface-bound GM_1. (A) The binding of the pentavalent CTB to a microsphere on which mobile receptors diffuse involves: (1) the transport of CT to the microsphere surface; (2) the binding of one of the five identical binding sites of the B-subunit of CTB to the carbohydrate moiety of a GM_1-receptor; and (3) the binding of free sites on CTB to additional receptors to form a CTB−receptor aggregate. This will lead to a distribution of bound complexes on the surface (B_1 through B_5). When receptors are confined to a surface, the transport of the ligand to the surface can influence the binding kinetics. In our binding experiments, transport of CTB to a surface of a microsphere is by diffusion. In analyzing data, we assume that $k_{+2} = k_{+3} = k_{+4} = k_{+5}$ and $k_{-1} = k_{-2} = k_{-3} = k_{-4} = k_{-5}$. (B) In the presence of GM_1-pentasaccharide, there are 10 additional surface states and 5 additional states in solution (not shown).

nistic description of the multivalent interaction of cholera toxin with GM_1 that is based on quantification of equilibrium binding and kinetic rate constants.

MATERIALS, METHODS, AND MODELING

Materials. CT, FITC-CTB, and gangliosides GM_1 and $GT1_b$ were from Sigma Chemical Co. (St. Louis, MO). All other gangliosides were from Matreya Inc. (Bellefonte, PA). GM_1 pentasaccharide salt was from Alexis Biochemicals (San Diego, CA). Phospholipids were from Avanti Polar Lipids (Alabaster, AL). Nonporous silica microspheres were purchased from Bangs Laboratories (Fishers, IN). 6-Carboxyfluorescein succinimidyl ester was from Molecular Probes (Eugene, OR). FITC-labeled calibration standards were from Flow Cytometry Standards Corp (San Juan, PR).

Preparation of Liposomes and Lipid-Coated Microspheres. Liposomes were prepared by depositing lipid mixtures as a thin film on the bottom of a glass tube by evaporating under a stream of nitrogen gas and resuspending in buffer by vortexing. The resulting multilamellar vesicle preparation was sonicated to clarity in a bath sonicator. Supported bilayers were formed by incubating liposomes with silica microspheres (2 μmol of lipid/1 $\times$ 10^7 microspheres) overnight at room temperature, followed by washing by three cycles of centrifugation and resuspension in buffer TES (50 mM Tris/1 mM EDTA/100 mM NaCl, pH 8.0). Incubation of samples was carried out for 30−60 min at 22 °C at a final concentration of 5×10^5 microspheres/mL in TES containing 0.1 mg/mL BSA (TSB) and followed by measurement of microsphere fluorescence by flow cytometry (*11*, *12*).

Preparation and Calibration of Fluorescent Ligands. Protein concentrations of toxin stock solutions were determined using the BioRad protein assay (Hercules, CA). Cholera toxin was labeled with 6-carboxyfluorescein succinimidyl ester. Fluoresceinated toxins were also measured by absorbance at 490 nm using an extinction coefficient of 8.1×10^4 M^{-1} cm^{-1}. Fluorescein stock solutions were measured by absorbance at 490 nm using an extinction coefficient of 7.25×10^4 M^{-1} cm^{-1}. Cuvette fluorescence measurements were made using a SPEX 1680 spectrofluorometer (Edison, NJ) and 1 cm square plastic cuvettes (Evergreen, Los Angeles, CA). Emission spectra were acquired and integrated and the buffer background subtracted using the SPEX Fluorolog software. The fluorophore-to-protein ratio (F/P) was found to be 4.3 and 1.4 for FITC-CTB and for 6-carboxyfluorescein-CT (FAM-CT), respectively. The quantum yields of fluorescent proteins relative to free fluorescein were determined by comparing fluorescence measurements of the absorbance-calibrated stock solutions and were 0.14 for FITC-CTB and 0.08 for FAM-CT.

Flow Cytometry. Flow cytometric measurements of microsphere fluorescence were made on a Becton-Dickenson FACSCalibur (San Jose, CA). Sample was illuminated at 488 nm (15 mW) and forward angle light scatter (FALS), 90° light scatter (side scatter, SSC), and fluorescence signals were acquired through a 530 (±30) nm band-pass filter. For kinetic measurements, time was also acquired from an internal clock in the data acquisition computer. Linear amplifiers were used for all measurements. Particles were gated on forward angle and 90° light scatter, and the mean fluorescence channel numbers were recorded. Kinetic experiments were started by measuring microsphere-supported bilayers in TSB buffer for ~8 s to establish a baseline. The sample tube was removed from the tube holder, CTB or CT was added at 10 s, the tube was vortexed, and sample was reintroduced into the instrument. The time between mixing and data acquisition was typically 10−20 s. The mean fluorescence channel number as a function of time was calculated using the IDLYK flow cytometry data analysis program (created at Los Alamos National Laboratory), and the amount of bound FITC-CTB or FAM-CT was calculated as described above. The time value for a given data point was the midpoint of the time window measured. Cytometric measurements (fluorescence channel) were calibrated in terms of mean equivalent soluble fluorescein molecules (MESF) using commercially available standardized FITC-labeled microspheres. The MESF per microsphere was converted to mean number of FITC-CTB or FAM-CT molecules per microsphere using the relative quantum yield of the fluorescent ligand relative to free fluorescein and the ratio of fluorophores per protein. The concentration of total toxin bound was calculated from the number of ligand molecules per microsphere and the microsphere concentration.

Data Analysis. Parameter estimates were obtained using a subroutine, DNLSI, from the Common Los Alamos Software Library, which is based on a finite-difference, Levenberg−Marquardt algorithm for solving nonlinear least-squares problems. Estimates of the standard deviations of the parameters were obtained by using a bootstrap method

(*13*). To obtain the estimates, each experiment was simulated 150 times.

Modeling. (A) Modeling the Interaction of CTB with Mobile GM$_1$-Receptors on a Spherical Surface. The binding of the pentavalent CTB to a microsphere on which mobile receptors diffuse involves the following: (1) the transport of CT to the microsphere surface; (2) the binding of one of the five identical binding sites of the B-subunit of CTB to the carbohydrate moiety of a GM$_1$-receptor; and (3) the binding of free sites on CTB to additional receptors to form a CTB−receptor aggregate. In general, this will lead to a distribution of bound complexes on the microsphere surface (B_1 through B_5).

When receptors are confined to a surface, the transport of the ligand to the surface can influence the binding kinetics. In our binding experiments, transport of CTB to a surface of a microsphere is by diffusion. We call D the diffusion coefficient of CTB in solution and k_{+1} and k_{-1} the fundamental forward and reverse rate constants, respectively, for the binding of a single binding domain of the B-subunit of CT to its receptor GM$_1$. k_{+1} and k_{-1} would be the single rate constants that would be determined in a binding experiment if the receptors were well mixed rather than confined to a surface. For a ligand diffusing to a microsphere which is large compared to the size of the ligand, the diffusion-limited forward rate constant equals $4\pi Da$, where a is the radius of the microsphere (*14*). One way to treat the transport step in the binding kinetics is to replace the true rate constants by the effective rate coefficients (*15*, *16*). For a pentavalent ligand binding to receptors on a microsphere of radius a, the effective forward and reverse rate coefficients, k_f and k_r, are

$$k_f = \frac{k_{+1}}{1 + \dfrac{5k_{+1}R}{4\pi Da}}$$

$$k_r = \frac{k_{-1}}{1 + \dfrac{5k_{+1}R}{4\pi Da}} \qquad (1)$$

where R is the free surface receptor concentration in receptors per microsphere. (Note that in eq 1 if R is given in receptors/microsphere, then k_{+1} is in cm^3/s, D in cm^2/s, and a in cm.)

In Figure 1, k_{+2} through k_{+5} are forward rate constants for aggregation. These rate constants involve reactions where both reactants are on a surface so that they have units of inverse surface concentration per second, e.g., cm^2 s^{-1}. When we fit kinetic data, we take $k_{+2} = k_{+3} = k_{+4} = k_{+5}$. It may be for steric, or other, reasons that the more sites that are bound on a CTB, the more difficult it is to bind additional receptors. This has been seen for a highly multivalent ligand binding to IgE on a cell (*17*, *18*). For the types of experiments we analyze, we cannot determine if the forward rate constants for aggregation differ. k_{-2} through k_{-5} are reverse rate constants for the opening of a bond an a CTB−receptor complex where 2 through 5 receptors are bound. In analyzing data, we assume that $k_{-1} = k_{-2} = k_{-3} = k_{-4} = k_{-5}$. It could be that when more receptors are bound to a single CTB, there is more strain on each bond in the complex so that $k_{-1} < k_{-2} < \ldots < k_{-5}$. Dissociation experiments at different ratios of CTB to GM$_1$ that will be presented suggest that if this occurs the differences in the dissociation rate constants are not large. There is evidence from solution binding studies that the binding of CTB to GM$_1$ may be cooperative with the binding of a GM$_1$ to a CTB subunit having a higher affinity when its neighboring subunit is bound (*4*). We have chosen not to add an additional parameter to our model in order to include cooperativity. The set of equations (eqs) that describes the binding kinetics, i.e., how the concentrations of the CTB−receptor aggregates change in time, are

$$\begin{aligned}
dB_1/dt &= 5k_fCR - k_rB_1 - 4k_{+2}B_1R + 2k_{-2}B_2\\
dB_2/dt &= 4k_{+2}B_1R - 2k_{-2}B_2 - 3k_{+3}B_2R + 3k_{-3}B_3\\
dB_3/dt &= 3k_{+3}B_2R - 3k_{-3}B_3 - 2k_{+4}B_3R + 4k_{-4}B_4\\
dB_4/dt &= 2k_{+4}B_3R - 4k_{-4}B_4 - k_{+5}B_4R + 5k_{-5}B_5\\
dB_5/dt &= k_{+5}B_4R - 5k_{-5}B_5
\end{aligned} \qquad (2)$$

The above eqs 1 and 2, plus the conservation laws for the total receptor concentration, R_T, and total ligand concentration, C_T, and eqs 3 and 4, make up the complete set of equations that are used to analyze the kinetic binding experiments. We use the conservation laws to eliminate C and R in eq 2 and then numerically solve these equations. The conservation equations are:

$$R_T = R + B_1 + 2B_2 + 3B_3 + 4B_4 + 5B_5 \qquad (3)$$

$$C_T = C + (factor)(B_1 + B_2 + B_3 + B_4 + B_5) \qquad (4)$$

where, if the CTB concentration is measured in nanomolar, the concentrations of the B_i in bound complexes per microsphere, and the concentrations of microspheres, p, in microspheres/mL, then $factor = p/(6.02 \times 10^{11})$. To calculate the fraction of bound CTB as in Figure 2A−C, we calculate $B/R_T = (B_1 + B_2 + B_3 + B_4 + B_5)/R_T$, by solving numerically eqs 2−4. Although one could obtain the equilibrium equations from eq 2 by setting the derivatives equal to zero, it is easier to write down these equations from Figure 1 using equilibrium thermodynamics. In terms of the equilibrium binding constant $K_1 = k_{+1}/k_{-1}$ and the equilibrium aggregation constant $K_2 = k_{+2}/k_{-2}$, we have that $B_1 = 5K_1CR$, $B_2 = (4/2)K_2RB_1$, $B_3 = (3/3)K_2RB_2$, $B_4 = (2/4)K_2RB_3$, and $B_5 = (1/5)K_2RB_4$. We analyze equilibrium binding experiments (Figure 2A) where B, the total concentration of bound CTB, is determined, so we wish to calculate this quantity. If we let $X = K_2R$, then

$$B = K_1CR(5 + 10X + 10X^2 + 5X^3 + X^4) \qquad (5)$$

The conservation laws can be rewritten in the following form:

$$R_T = R + K_1CR(5 + 20X + 30X^2 + 20X^3 + 5X^4) \qquad (6)$$

$$C_T = C + (factor)K_1CR(5 + 10X + 10X^2 + 5X^3 + X^4) \qquad (7)$$

(Recall that *factor* is defined after eq 4.) Using eq 7 to eliminate C in eq 6, we obtain

$$R_T = R + \frac{K_1C_TR(5 + 20X + 30X^2 + 20X^3 + 5X^4)}{1 + (factor)K_1R(5 + 10X + 10X^2 + 5X^3 + X^4)} \qquad (8)$$

Since $X = K_2R$, eq 8 is an equation with one unknown, R, that we can solve numerically. Once we know R, we determine C from eq 7, and then, knowing R and C, we calculate B, the experimentally measured quantity. This is how we calculate B when we fit our equilibrium binding data in Figure 2A.

(B) Modeling the Competition of Soluble Receptors (GM_1-Pentasaccharide) with GM_1-Receptors on a Spherical Surface. This describes the analysis of the inhibition experiments (Figure 2B) where a soluble receptor, GM_1-pentasaccharide, is used to compete with receptors, GM_1, on microspheres for CTB binding sites. We will use the notation that B_{ij} is the concentration of bound CTB on the surface with i surface receptors bound and j soluble receptors bound. The 15 possible states of surface-bound CTB are shown in Figure 1B. Not shown are the five states of CTB in solution, CTB with no sites bound, CTB with one site bound to soluble receptor, CTB with two sites bound to soluble receptor, etc. We call the equilibrium constant for the binding of a GM_1-pentasaccharide to a single site on CTB K_s. If the binding to CTB is the same for a surface GM_1 and a GM_1-pentasaccharide, then $K_s = K_1$; however, we found this not to be the case. One can show that in the presence of soluble receptor the form of eq 8 is unchanged but K_1 and K_2 are replaced by $\bar{K}_1 = K_1/(1 + K_sS)$ and $\bar{K}_2 = K_2/(1 + K_sS)$ where S is the concentration of free soluble receptor. For the inhibition experiments we analyze, there is negligible depletion of soluble receptor, so we take $S = S_T$, the total GM_1-pentasaccharide concentration. Equations 6 and 7 become

$$R_T = R + (1 + K_1S)^5\bar{K}_1CR(5 + 20\bar{X} + 30\bar{X}^2 + 20\bar{X}^3 + 5\bar{X}^4) \quad (9)$$

$$C_T = [(1 + K_1S)^5] \times [C + (factor)\bar{K}_1CR(5 + 10\bar{X} + 10\bar{X}^2 + 5\bar{X}^3 + \bar{X}^4)] \quad (10)$$

where $\bar{X} = \bar{K}_2R$. Now we can proceed as in part (A) to calculate the bound concentration.

RESULTS

Quantitative Measurement of Equilibrium Binding of CTB to Its Ganglioside Receptor GM_1 by Flow Cytometry. Binding of fluorescently labeled cholera toxin B subunit (FITC-CTB) to ganglioside GM_1 present in bilayer membranes supported on glass microspheres was measured quantitatively using flow cytometry. Flow cytometry allows the sensitive and quantitative measurement of interactions, and its inherent discrimination of free and bound fluorescence allows one to analyze these interactions with continuous kinetics as well as at equilibrium. Specific equilibrium binding of FITC-CTB to microsphere-supported bilayers containing 0.5 mol % GM_1 shows characteristic saturation and half-maximal binding at $\sim 5 \times 10^{-9}$ M (Figure 2A). Because binding between FITC-CTB and GM_1 is multivalent, the concentration at which half-maximal binding occurs does not represent the equilibrium dissociation constant K_D, an approximation often used for single-site interactions. Rather, the half-maximal binding concentration represents a semiquantitative description of binding avidity resulting from the multivalent interaction of CT with receptor. At saturation in the binding curve (total concentration of FITC-CTB is between 2×10^{-8} and 4×10^{-8} M), only about 2×10^{-10} M FITC-CTB is bound to microspheres (Figure 2A). Since the amount bound to microspheres is at most only ~1% of the total concentration of FITC-CTB, we can rule out that depletion of FITC-CTB is contributing to the plateau in the curve. In buffer

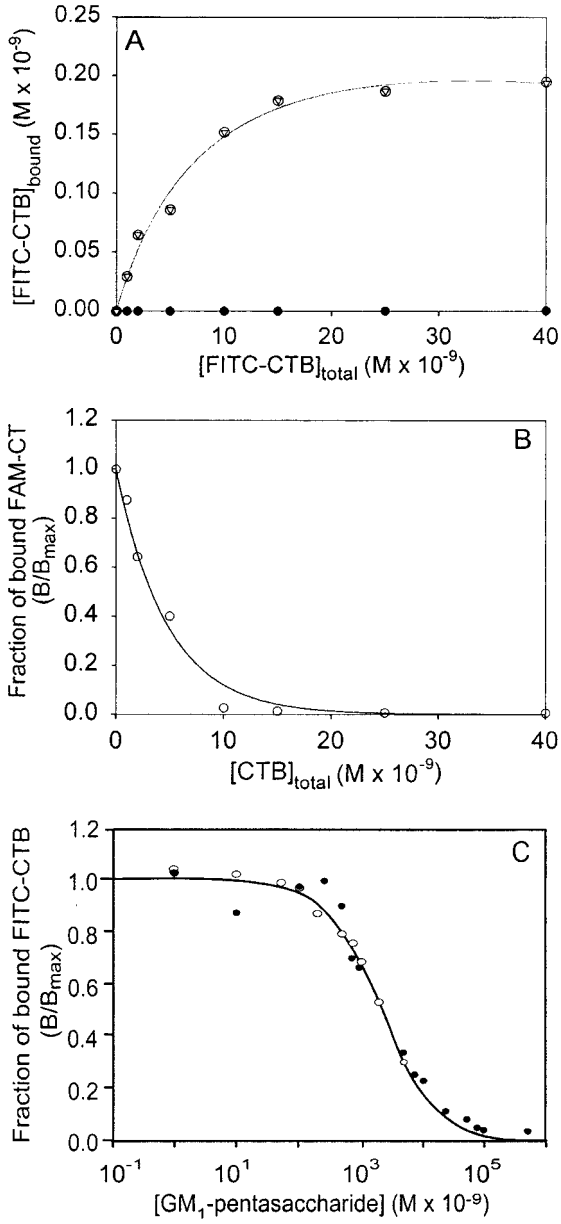

FIGURE 2: Interactions of FITC-CTB with GM_1. (A) Equilibrium binding of $(0-40) \times 10^{-9}$ M FITC-CTB to microsphere-supported bilayers containing 0.5 mol % GM_1 (sample incubation 60 min at 22 °C). Open circles = total binding, closed circles = nonspecific binding, triangles = specific binding (difference between total and nonspecific binding). (B) Competitive binding of unlabeled CTB. Microsphere-supported bilayers containing 0.5 mol % GM_1 were preincubated with $(0-40) \times 10^{-9}$ M unlabeled CTB (30 min, 22 °C) followed by incubation with saturating concentrations of FITC-CTB (20×10^{-9} M, 30 min, 22 °C). (C) Competitive binding of GM_1-pentasaccharide. Preincubation of supported bilayers containing 0.5 mol % GM_1 with $(0-1) \times 10^{-3}$ M GM_1-pentasaccharide salt for 30 min at 22 °C followed by 20×10^{-9} M FITC-CTB for 30 min at 22 °C. Closed and open circles indicate two different experiments. (A−C) Lines represent fits. Fit for panel A was obtained by solving eq 8 numerically and then using eqs 5 and 6. The line in panel B represents fit to the equation $y = ae^{-bx}$. Fit for panel C was obtained by solving eqs 9 and 10 and then using eq 5 with X replaced by $\bar{X}$.

containing low concentrations of albumin (0.1 mg/mL), nonspecific binding as determined in the presence of excess free unlabeled CTB (Figure 2A) or using bilayers containing no GM_1 (data not shown) is low. When microsphere-supported bilayers were preincubated with varying concentrations of unlabeled CTB before they were incubated with 2×10^{-8} M FITC-CTB (a concentration corresponding to saturation in the binding curve, see Figure 2A), we found half-maximal binding of CTB at a similar concentration (Figure 2B). This indicates that the effect of the fluorophore on toxin binding is negligible. The requirement for labeling of CTB might seem to present a disadvantage compared to label-free methods, such as SPR, but the label has no effect on binding of CTB to GM_1 and enables us to detect binding of FITC-CTB at much lower receptor densities (0.01 mol %, ~5000 FITC-CTB molecules/microsphere) than possible by SPR.

Single-Site Interaction of a CTB Binding Domain with a GM_1-Receptor. A realistic model requires consideration of the monovalent interaction of a single FITC-CTB binding site with one GM_1-receptor. Competition of soluble GM_1-pentasaccharide salt with FITC-CTB revealed half-maximal inhibition to be $\sim 2 \times 10^{-6}$ M (Figure 2C), providing an estimate for the apparent affinity of the monovalent GM_1−CTB interaction. This is ~400-fold weaker than the apparent avidity observed for the pentameric interaction (half-maximal binding at $\sim 5 \times 10^{-9}$ M, Figure 2A), which reflects the contributions of both monovalent binding and cross-linking. Similar large avidity effects have been predicted and observed for bivalent IgG and pentavalent IgM with the intact antibodies having apparent affinities 10^1-10^3-fold larger than their Fab fragments (*19*−*21*). When this inhibition curve (Figure 2C) and the equilibrium binding curve (Figure 2A) were simultaneously fit, we obtained the following equilibrium constants: (a) equilibrium binding constant for GM_1 and a single subunit of FITC-CTB, $K_1 = (8.0 \pm 2.9) \times 10^7$ M^{-1}; (b) equilibrium binding constant for the soluble GM_1-pentasaccharide to a site on FITC-CTB, $K_s = (3.7 \pm 1.3) \times 10^6$ M^{-1}; and (c) a maximal value for the cross-linking constant, $K_2 = 2.4 \times 10^{-13}$ cm^2. Surprisingly, we found that the equilibrium binding constant for FITC-CTB binding monovalently to GM_1 is ~20-fold higher compared to the one for monovalent binding to soluble GM_1-pentasaccharide. A good fit could not be obtained when $K_1 = K_s$ (see modeling of competition of soluble receptors with GM_1-receptors on a spherical surface). The difference between K_1 and K_s is probably due to a preferred presentation of the polysaccharide receptor by membrane-bound GM_1 compared to free receptor in solution.

Dissociation Kinetics of FITC-CTB from GM_1-Bearing Supported Bilayers. Because of its intrinsic discrimination between free and particle-associated (bound) fluorescence, flow cytometry is able to make sensitive and quantitative measurements of molecular interactions with continuous kinetic resolution. Since the stability of an interaction is most directly revealed in its dissociation kinetics, we initiated dissociation of bound FITC-CTB by the addition of excess CTB. Because the dissociation kinetics are expected to depend on the valency of CTB-GM_1 binding, we prepared samples with a constant concentration of GM_1 and different concentrations of FITC-CTB (0.1×10^{-9}, 0.5×10^{-9}, 1×10^{-9}, and 20×10^{-9} M). At a low initial concentration of

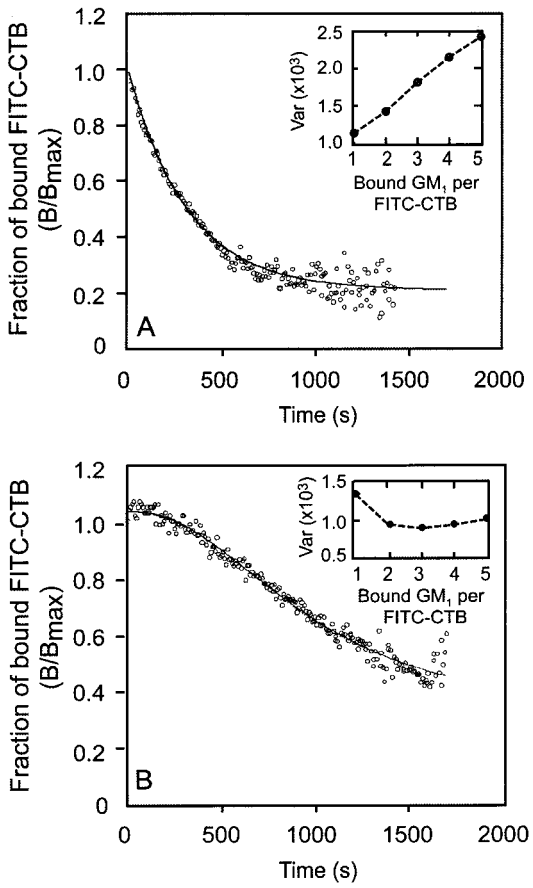

FIGURE 3: Dissociation kinetics of FITC-CTB from GM_1-containing supported bilayers. Supported bilayers containing 0.5 mol % GM_1 were incubated with 20×10^{-9} M (A) or 0.5×10^{-9} M (B) FITC-CTB for 30 min at 22 °C, followed by addition of 1×10^{-6} M CTB and measurement of dissociation of CTB by flow cytometry. The insets of (A) and (B) show the variance (Var) of these fits at an intial low [20×10^{-9} M FITC-CTB, (A)] and high ligand concentration [0.5×10^{-9} M FITC-CTB, (B)]. A minimum in the variance indicates the most prevalent number of GM_1 bound per FITC-CTB. The dissociation curves are fit with the expression $B = 1 - (1 - e^{-k_1 t})^N$. This formula predicts the fraction of CTB that remains bound at time t if at the start of the experiment all the CTB are in the same state with N sites bound, and if a GM_1 that dissociates from a CTB binding site immediately binds to a site on an unlabeled CTB (*32*). Shown in (A) is the fit for $N = 1$ and in (B) the fit for $N = 3$. Each dissociation curve was fit for $N = 1$ through $N = 5$.

FITC-CTB, GM_1-receptors are in excess, and we expect the pentavalent toxin to bind with maximal valency. As the concentration of FITC-CTB increases, we expect the average number of GM_1 bound per FITC-CTB to decrease, as CTB competes for receptor.

Presented in Figure 3A and Figure 3B are the dissociation kinetics for FITC-CTB at an initial concentration of 20×10^{-9} and 0.5×10^{-9} M, respectively, from supported bilayers (0.5 mol % GM_1). At a high initial concentration of 20×10^{-9} M FITC-CTB (Figure 3A), we could fit the dissociation curve with a single exponential and determined a dissociation rate constant k_{-1} of $(3.21 \pm 0.03) \times 10^{-3}$ s^{-1}. This parameter value is independent of the details of the model for CTB binding. To obtain an accurate value for k_{-1} requires only that the FITC-CTB/GM_1 ratio is sufficiently high, that CTB is bound to only one GM_1 at the start of the experiment, and that the concentration of unlabeled CTB added to initiate dissociation is high enough to block rebinding. At a constant

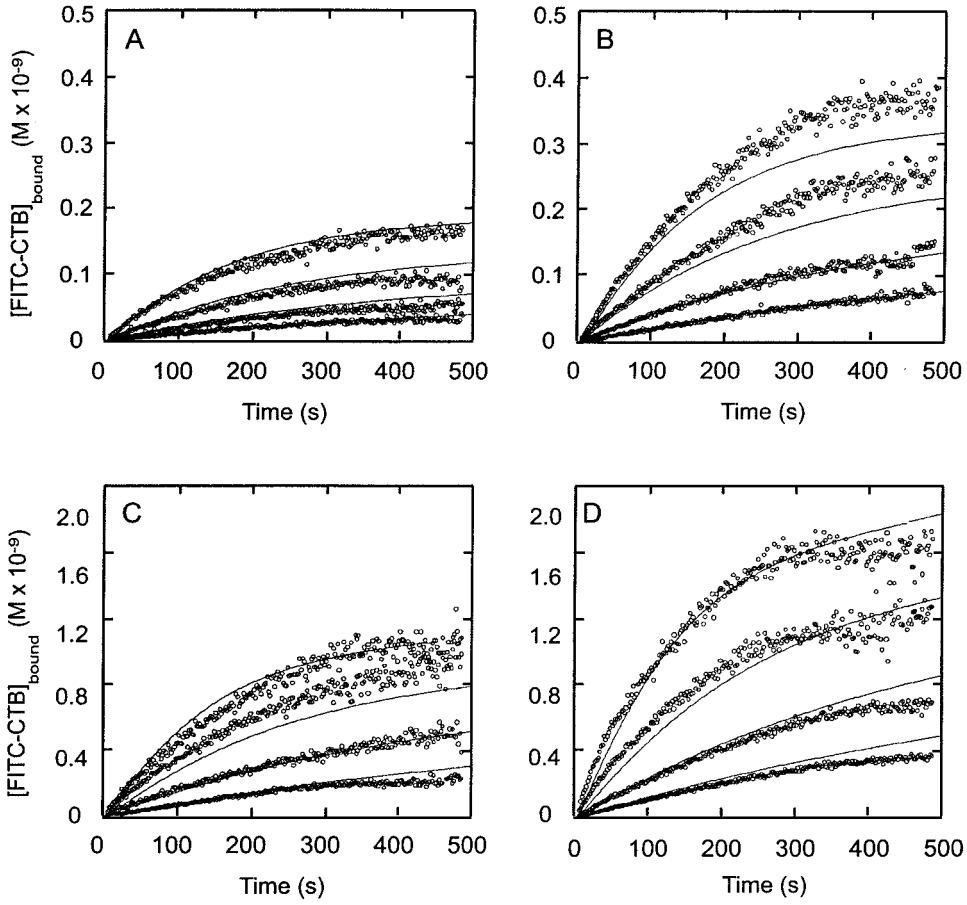

FIGURE 4: Kinetics of binding of FITC-CTB to GM_1-containing supported bilayers. Supported bilayers containing 0.01 (A), 0.05 (B), 0.1 (C), or 0.5 (D) mol % GM_1 were incubated with 2.5×10^{-9} (first plot from bottom), 5×10^{-9} (second plot from bottom), 10×10^{-9} (third plot from bottom), or 20×10^{-9} M (fourth plot from bottom) FITC-CTB, and binding of FITC-CTB was monitored over time. Lines represent the fits of these curves by solving eqs 1−4 numerically. All curves and two additional binding curves for nonspecific binding were fitted simultaneously. The simultaneous fitting reduces the maximal overlap between an individual curve and its fit.

receptor density, the shape of the dissociation curve exhibited a marked dependence on the initial concentration of FITC-CTB (for 20×10^{-9} and 0.5×10^{-9} M, see Figure 3A,B; for 1×10^{-9} and 0.1×10^{-9} M, data not shown). The occurrence of an initial lag phase in the dissociation kinetics becomes more and more extended as the initial concentration of FITC-CTB is lowered. This lag reflects the time needed to open up increasing numbers of bonds between FITC-CTB and GM_1-receptors before dissociation can occur. At low initial concentrations of FITC-CTB, receptors are in excess, and the average number of GM_1 bound per toxin will be maximal. At sufficiently high concentrations of FITC-CTB, where toxin molecules must compete for receptors, the lag phase disappears, dissociation becomes single-exponential, and only a single GM_1 is bound per CTB (inset, Figure 3A). Our results at an initial concentration of 0.5×10^{-9} M FITC-CTB indicate that the dominant binding state is 3 GM_1 per toxin, but coexists with those of 1, 2, 4, and 5 receptors (inset Figure 3B). In Figure 3B, the best fit is obtained for $k_{-1} = (1.7 \pm 0.09) \times 10^{-3}$ s^{-1}, which is approximately a factor of 2 smaller than the value for k_{-1} in Figure 3A. A single CTB−GM_1 bond appears to open more slowly when additional bonds are present, and this is consistent with cooperative binding (*4*).

Kinetics of Association of CTB with GM_1 in Supported Bilayers. To obtain the forward rate constant, we simultaneously fit 16 curves for association of FITC-CTB at 4 different concentrations (2.5×10^{-9}, 5×10^{-9}, 10×10^{-9}, or 20×10^{-9} M) to supported bilayers containing GM_1 at four different concentrations (0.01, 0.05, 0.1, and 0.5 mol %; Figure 4A−D) and two additional curves for nonspecific binding to surfaces containing no GM_1 (data not shown). We determined (a) an association rate constant k_{+1} of $(3.4 \pm 0.6) \times 10^4$ M^{-1} s^{-1}, (b) a dissociation rate constant k_{-1} of $(1.9 \pm 0.6) \times 10^{-3}$ s^{-1}, a value similar to the one determined directly from the dissociation kinetics [$(3.21 \pm 0.03) \times 10^{-3}$ s^{-1}], and (c) a cross-linking constant K_2 of $(9.3 \pm 3.3) \times 10^{-13}$ cm^2, which is slightly higher than the maximum K_2 determined from simultaneously fitting the curves for equilibrium binding and inhibition with soluble GM_1-pentasaccharide (2.4×10^{-13} cm^2). If in the simultaneous fit we fix k_{-1} to 3.21×10^{-3} s^{-1}, the value determined directly from the dissociation kinetics, we obtain the following values for $k_{+1} = (2.8 \pm 0.4) \times 10^4$ M^{-1} s^{-1} and $K_2 = (1.1 \pm 0.1) \times 10^{-12}$ cm^2. In our model, we assume that $k_{-2} = k_{-1}$, allowing us to derive the cross-linking rate constant: $k_{+2} = K_2 k_{-1} = 3.53 \times 10^{-15}$ cm^2 s^{-1}. This value corresponds to a singly bound CTB cross-linking a second GM_1 where the two bound GM_1 are not nearest neighbors. When the cross-linking is to a nearest neighbor, k_{+2} will be larger by a factor of 2−4 because of cooperativity; i.e., for nearest neighbors, $k_{-1} > k_{-2}$ (*4*).

Interaction of CT with GM_1 Is of Higher Avidity than That of the B-Subunit Alone. We also examined the interaction

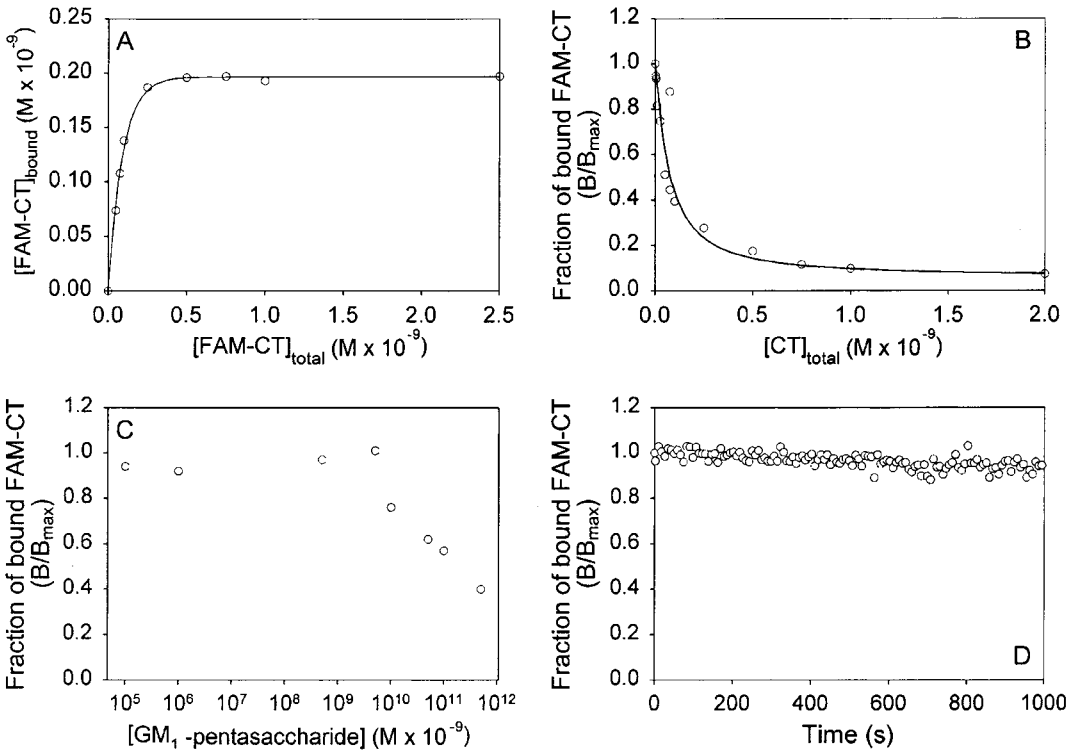

FIGURE 5: Interactions of FAM-CT with GM_1. (A) Specific equilibrium binding of $(0-5) \times 10^{-9}$ M FAM-CT to supported bilayers containing 0.5 mol % GM_1 (sample incubation 60 min at 22 °C). Line represents fit to the equation $y = a(1 - e^{-bx})$ to obtain a value for half-maximal binding. (B) Competitive binding of unlabeled CT. Microsphere-supported bilayers containing 0.5 mol % GM_1 were preincubated with $(0-5) \times 10^{-9}$ M unlabeled CT (30 min, 22 °C) followed by incubation with saturating concentrations of FAM-CT (5×10^{-9} M, 30 min, 22 °C). The line represents fit to the equation $y = ae^{b/x+c}$. (C) Competition of GM_1 with GM_1-pentasaccharide. Preincubation of supported bilayers containing 0.5 mol % GM_1 with 0−0.01 M of GM_1-pentasaccharide for 30 min at 22 °C followed by 5×10^{-9} M FAM-CT for 30 min at 22 °C. (D) Dissociation kinetics of FAM-CT. Incubation of supported bilayers containing 0.5 mol % GM_1 with 20×10^{-9} M FAM-CT for 5 min at 22 °C, followed by addition of 1×10^{-6} M CT and measurement of dissociation of CT by flow cytometry.

of whole cholera toxin (CT = A- and B-subunits) with GM_1-bearing supported bilayers. Representative specific equilibrium binding of FAM-CT to supported bilayers containing 0.5 mol % GM_1 is shown in Figure 5A. As for FITC-CTB, the nonspecific binding of FAM-CT in the presence of excess unlabeled cholera toxin or to bilayers without GM_1 is low (data not shown). At saturation, the concentration of specifically bound FAM-CT on a microsphere was $\sim 2 \times 10^{-10}$ M and similar to that of FITC-CTB ($\sim 2 \times 10^{-10}$ M, Figure 2A). Half-maximal binding was found to occur at $\sim 5 \times 10^{-11}$ M (Figure 5A), a concentration ~100-fold lower than the one observed for FITC-CTB (Figure 2A). Competition of FAM-CT with CT is shown in Figure 5B and resulted in half-maximal inhibition at $\sim 5 \times 10^{-11}$ M. Taken together, this indicates that binding between the whole toxin and GM_1 is of ~100-fold higher avidity than binding between the B-subunit and GM_1.

Half-maximal inhibition of the monovalent interaction of one GM_1 with one B-subunit of CT was observed at $\sim 1 \times 10^{-3}$ M GM_1-pentasaccharide (Figure 5C), a concentration ~500-fold higher than required for inhibition of FITC-CTB ($\sim 2 \times 10^{-16}$ M, Figure 2C). This suggests that the stronger binding of the whole toxin compared to the B-subunit alone is due to an increase in K_1, the affinity of a B-subunit binding site for GM_1.

The significantly lower concentration of FAM-CT required to reach half-maximal binding compared to the B-subunit alone suggests that dissociation of the whole toxin occurs at a slower rate than that of the B-subunit. At the same initial concentration (20×10^{-9} M FAM-CT or FITC-CTB), we determined that the half-time for dissociation from 0.5 mol % GM_1 in supported bilayers is ≫1000 s for the whole toxin (Figure 5D) and ~400 s for the B-subunit (Figure 3A). In contrast to FITC-CTB, dissociation of FAM-CT does not appear to depend on the initial concentration of FAM-CT between 0.1×10^{-9} and 20×10^{-9} M (shape of curve and half-time did not change, data not shown). Also, the half-time did not change when dissociation was induced from supported bilayers containing 0.05, 0.1, or 0.5 mol % GM_1 (data not shown), indicating insensitivity to receptor concentration over this range. The almost complete lack of dissociation at various receptor/ligand ratios indicates that the whole toxin binds significantly tighter than the B-subunit.

Interaction of CTB and CT with Gangliosides Other than GM_1. Over the concentration range tested [$(0-50) \times 10^{-9}$ M], FITC-CTB and FAM-CT did not show detectable binding to supported bilayers containing any other glycosphingolipid (GM_2, GM_3, $GD1_a$, $GD1_b$, $GT1_b$, asialo-GM_1, GL4 globoside, lactosyl ceramide) at 0.5 mol % (data not shown). Because of the importance of receptor concentration for multivalent binding, we repeated our measurements with supported bilayers containing 5 mol % of these glycosphingolipids. We observed low but specific binding of FITC-CTB and FAM-CT only to $GD1_b$ and asialo-GM_1 (data not shown). Figure 6A shows representative specific equilibrium binding of FITC-CTB to supported bilayers containing 5 mol % $GD1_b$ or asialo-GM_1. At this receptor surface density, binding of FITC-CTB to $GD1_b$-bearing surfaces was found

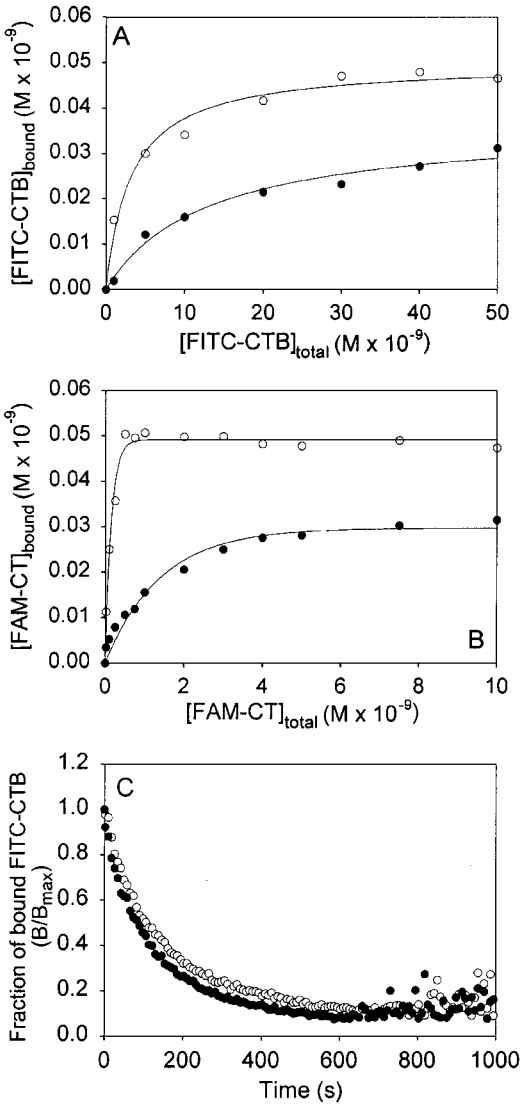

FIGURE 6: Interactions of FITC-CTB and FAM-CT with $GD1_b$ and asialo-GM_1. (A) Specific equilibrium binding of $(0-40) \times 10^{-9}$ M FITC-CTB to supported bilayers containing 5 mol % $GD1_b$ (open circles) or 5 mol % asialo-GM_1 (closed circles). Sample incubation 60 min at 22 °C. Lines represent fits to the equation $y = x/a + bx$. (B) Specific equilibrium binding of $(0-10) \times 10^{-9}$ M FAM-CT to supported bilayers containing 5 mol % $GD1_b$ (open circles) or 5 mol % asialo-GM_1 (closed circles). Sample incubation 60 min at 22 °C. Lines represent fits to the equation $y = a(1 - e^{-bx})$. (C) Dissociation kinetics from supported bilayers containing 5 mol % $GD1_b$ (open circles) or asialo-GM_1 (closed circles). Supported bilayers containing $GD1_b$ or asialo-GM_1 were incubated with 20×10^{-9} M FITC-CTB for 30 min at 22 °C, followed by addition of 1×10^{-6} M CTB and measurement of dissociation of CTB by flow cytometry.

to be somewhat stronger (i.e., the total levels of binding were ~2-fold higher, and the binding curve was steeper in the low concentration range; Figure 6A) compared with binding to surfaces bearing asialo-GM_1. At saturation, specific binding of FITC-CTB to microspheres containing 5 mol % $GD1_b$ or asialo-GM_1 was ~4- and 8-fold lower (Figure 6A) compared to microspheres bearing 0.5 mol % GM_1 ($\sim 2 \times 10^{-10}$ M, Figure 2A). Specific equilibrium binding of FAM-CT to supported bilayers containing 5 mol % $GD1_b$ or asialo-GM_1 is shown in Figure 6B. While we observe the same order of binding strength as for FITC-CTB ($GM_1 \gg GD1_b > $ asialo-GM_1), we find that saturation occurs at lower concentrations. Half-maximal binding of FAM-CT to $GD1_b$ occurs at $\sim 1 \times 10^{-10}$ M and to asialo-GM_1 at $\sim 1 \times 10^{-9}$ M (Figure 6B) compared with half-maximal binding of FITC-CTB at $\sim 4 \times 10^{-9}$ and 9×10^{-9} M, respectively (Figure 6A). Thus, the stronger binding of the whole toxin compared to the pentameric B-subunit does not appear to be receptor-dependent.

The high receptor concentrations required to support binding of FITC-CTB or FAM-CT to $GD1_b$ and asialo-GM_1 indicate that the avidity of the B-subunit or the whole toxin for these two gangliosides is considerably lower than theavidity for GM_1. This suggests that the stability of the toxin−receptor interaction is much lower for bilayers containing $GD1_b$ or asialo-GM_1 compared to those containing GM_1 that is expected to manifest in a decreased half-time for dissociation and an increased k_{-1}. As predicted, FITC-CTB dissociates much faster from supported bilayers containing 5 mol % $GD1_b$ or asialo-GM_1 ($t_{1/2}$ <200 s, Figure 6B) than from bilayers containing 0.5 mol % GM_1 ($t_{1/2}$ ~400 s, Figure 3A). Consistent with our binding data, we also find that FITC-CTB dissociates somewhat slower from supported bilayers containing $GD1_b$ ($t_{1/2} \sim 120$ s, Figure 6C) compared to those containing asialo-GM_1 ($t_{1/2}$ ~100 s, Figure 6C).

DISCUSSION

Development of a Multistep Model for Recognition of GM_1 by Cholera Toxin. Our main goal was to understand the mechanism of the multivalent interaction of CT with its ganglioside receptor GM_1 in detail. Previous kinetic studies describing the interaction of CT with GM_1 relied on simple single-site binding models that ignore receptor cross-linking, and therefore do not address the multistep feature of CT binding (*5*−*8*). We have developed a multistep model (Figure 1) that takes into account receptor cross-linking. The first step in the model is the diffusion-limited transport of the pentameric CTB to the surface of a microsphere. At the surface of the microsphere, pentameric CTB initially binds with an effective forward rate constant k_f to the carbohydrate moiety of one GM_1 molecule in the membrane. Upon this initial single-site binding step, the CTB can either dissociate from this GM_1 with an effective reverse rate constant k_r (corrected for surface density of R) or bind to a second GM_1 molecule with a cross-linking rate constant k_{+2}. This cross-linking step depends on the concentration of GM_1 in the membrane and its rate of lateral diffusion. It can be repeated up to 4 times. At low concentrations of FITC-CTB, if the GM_1 concentration is sufficiently high and the equilibrium cross-linking constant sufficiently large, all five binding sites on CTB will be occupied by GM_1-receptors, resulting in a pentavalent, high-avidity, binding of CTB to the membrane. In our model, we have taken $k_{+2} = k_{+3} = k_{+4} = k_{+5}$ and $k_{-1} = k_{-2} = k_{-3} = k_{-4} = k_{-5}$ (*22*). A much more elaborate study would be required to determine if all the forward and all the reverse rate constants are equal. Making these assumptions and then using the model to fit the data and determine average values for the parameters is a first step in quantifying the aggregation process.

Equilibrium solution binding studies have suggested GM_1 binds cooperatively to CTB with a modest increase (a factor of 4) in the affinity for GM_1 for a CTB subunit when the bonds are adjacent (*4*). We did not include cooperativity in

the model, but our dissociation studies (Figure 3A,B) are consistent with such cooperative binding. We expect that cooperstivity would result in small differences in the forward rate constant as well.

Receptor Cross-Linking Occurs at a Slow Rate. It appears that cross-linking is slow ($k_{+2} = 1.8 \times 10^{-15}$ cm^2 s^{-1}). For significant receptor aggregation to occur (see Figure 1A), i.e., for CTB to bind more than one GM_1, $4k_{+2}R_T > 2k_{-1}$ or equivalently $2K_2R_T > 1$ (*17*, *23*). If the GM_1 concentration is sufficiently high, then at low concentrations of FITC-CTB a FITC-CTB with one site bound will have a high probability of binding to a second GM_1 before it dissociates. We have determined that $K_2R_T = 1.4 \pm 0.5$. Therefore, at low concentrations of CTB, we expect more than one GM_1 bound per toxin as was inferred in Figure 3B. The lateral diffusion coefficient of GM_1 incorporated into preformed dimyristoylphosphatidylcholine vesicles above the gel−liquid-crystalline transition temperature has been determined to be $\sim 5 \times 10^{-9}$ cm^2 s^{-1} and was found to be independent of the GM_1 concentration between 1 and 10 mol % (*24*). Thus, under our conditions, the rate of cross-linking is well below the diffusion limit, which is expected to be $\sim 3.6 \times 10^{-8}$ cm^2 s^{-1}.[2] The 3-dimensional forward rate constant k_{+2} is well below its diffusion limit, and in two dimensions, there may be additional steric hindrance that further reduces k_{+2}. Very few values for rate constants for cross-linking have been determined. In a well-studied case, the cross-linking by bivalent ligands of IgE that are complexed with FceRI on the surface of rat basophilic leukemia (RBL) cells, k_{+2} is also well below the diffusion limit (*17*, *23*).

At our GM_1 concentration of 0.01−0.5 mol %, we have $\sim 1 \times 10^5$ to 5×10^6 receptors on a microsphere. This corresponds to $\sim 1.3 \times 10^{11}$ to 6.4×10^{12} GM_1-receptors/cm^2. A RBL cell expresses $(3-6) \times 10^5$ IgE receptors per cell (*19*). Assuming a surface area of 5×10^{-6} cm^2 for an RBL cell, this corresponds to an average of $\sim 6 \times 10^{10}$ IgE receptors/cm^2. Therefore, compared to a protein receptor on a cell surface, we have a ∼100-fold higher concentration of GM_1-receptors on our microspheres. The high concentration of GM_1 is probably physiologically relevant since it is known that a large fraction of GM_1 concentrates in detergent-resistant lipid microdomains of the plasma membrane. Indeed, a recent study that used chimeras of subunits of CT and *E. coli* heat-labile type II enterotoxin showed that the function of CT in polarized intestinal epithelial cells critically depends on binding/clustering specifically GM_1 to purposely sort the GM_1−toxin complexes into detergent-resistant lipid microdomains (*25*, *26*).

Kinetics of Association of FITC-CTB with GM_1. An association rate constant of 6.2×10^5 M^{-1} s^{-1} has been reported using SPR and GM_1 at 0.04, 0.4, or 0.8 mol % (*7*, *8*). Since we define k_{+1} as the forward rate constant for a single site on a B-subunit to interact with GM_1, the forward rate constant for the whole B-subunit would be $5k_{+1}$ ($\sim 1.7 \times 10^5$ M^{-1} s^{-1}), which is ∼4-fold lower than determined by SPR (*7*, *8*). In these studies, K_D's of 2.6×10^{-10} and 7.3×10^{-10} M were derived simply by dividing the kinetic rate constants for dissociation (1.6×10^{-4} s^{-1} and 4.5×10^{-4} s^{-1}) and association (*7*, *8*). These are not true equilibrium constants, however, and will depend on the receptor densities used. Indeed, it was observed that the slope of the Scatchard plot changed with the GM_1 concentration (*7*).

Comparison to Studies Using SPR. The immobilization of GM_1 to the various sensor chip surfaces used in SPR studies was accomplished by different means. The K sensor chip used by Kuziemko et al. (*6*) has a self-assembled alkylthiol layer on its gold surface, and after adding liposomes containing GM_1, a hybrid bilayer is formed. MacKenzie et al. (*7*) used a CM5 sensor chip that contains carboxylated dextran on its surface to which they covalently linked an anti-LPS antibody. To anchor the GM_1, they incubated with liposomes that contain low amounts of LPS and GM_1. It is not clear whether these liposomes actually have sufficient lateral mobility required for receptor aggregation. A newly developed L1 sensor chip was used by Cooper et al. (*8*). This sensor chip has a lipophilic dextran on its surface on which a bilayer is formed after incubation with liposomes containing GM_1. It is expected that the ability of CT to aggregate GM_1 will depend strongly on the way GM_1 is coupled to the sensor surface. To obtain intrinsic forward and reverse rate constants of the ligand−receptor reaction from an SPR experiment therefore requires modeling that accounts for transport processes of diffusion and flow to the and within the sensor surface (*27*).

Binding of Whole Toxin Is Stronger than Binding of the B-Subunit Alone. Our results consistently show that the interaction of the whole toxin with GM_1 is of considerably higher avidity than that of the B-subunit alone. The pentameric B-subunit is responsible for binding to GM_1-receptors in the apical face of intestinal epithelial cell membrane and assists the A-subunit in translocating through the membrane where it then ADP-ribosylates a heterotrimeric G-protein. No previous study has quantitatively compared the thermodynamics of interaction of the B-subunit with those of the whole toxin. It has been suggested from the structural data (*28*) and accessibility studies with antibodies defining the orientation of CT with respect to the cell membrane (*29*, *30*) that the A2-subunit may interact with the membrane surface during binding of the B-subunit to GM_1. Our data on the ∼100-fold increased avidity of the whole toxin compared to the B-subunit suggest that this indeed the case. This additional interaction of the A2-subunit with the membrane could reduce k_{-1} and/or increase k_{+2}, leading to a stronger binding of the whole toxin compared to CTB.

Interaction of CTB and CT with $GD1_b$ and Asialo-GM_1 Requires High Receptor Concentrations. Our data on the interaction of CTB or CT with a battery of glycosphingolipids (GM_1, GM_2, GM_3, $GD1_a$, $GD1_b$, $GT1_b$, asialo-GM_1, GL4 globoside, lactosyl ceramide) at a concentration of 0.5 mol % revealed that the B-subunit as well as the whole toxin exclusively bind to GM_1. A ∼10-fold higher K_D (derived from the ratio of reverse and forward kinetic rate constants determined by SPR) for the interaction between CTB with $GD1_b$ compared to the interaction with GM_1 was reported using 0.8 mol % GM_1 or $GD1_b$ (*7*). This difference in K_D's was due to ∼10-fold higher k_{-1} for the weak interaction of CTB with $GD1_b$ (*7*). However, for a weak interaction, a

[2] The diffusion limit of the forward rate constant, k_{+2}, calculated under the assumption that both the unbound GM_1 and the toxin−GM_1 cluster diffuse in the bilayer with the same two-dimensional diffusion coefficient, D, has the form: $k_{+2} = -8\pi D/[\ln(4A) + 0.46]$, where A is the fraction of the surface area occupied by GM_1 (*1*). This result was obtained by assuming that A is small. For $D = 5 \times 10^{-9}$ cm^2 s^{-1} and $A = 0.005$, $k_{+2} = 3.64 \times 10^{-8}$ cm^2 s^{-1}.

higher receptor surface density is required for efficient cross-linking to occur before CTB dissociates. Because of the importance of the receptor concentration, we also examined the interaction of CTB and CT with these glycosphingolipids at a receptor density of 5 mol % and found that CTB and CT bind in the same relative order to $GM_1 \gg GD1_b >$ asialo-GM_1. Kuziemko et al. measured the binding of CT to a battery of gangliosides by SPR, and they report that 5 mol % was the lowest concentration of ganglioside that gave analyzable kinetic data (*6*). They determined the following order of binding affinities for CT: $GM_1 > GM_2 > GD1_a > GM_3 > GT1_b > GD1_b >$ asialo-GM_1, and nonspecific binding occurring to globoside and lactosyl ceramide only. At this high receptor concentration, they derive a K_D of 4.6×10^{-12} M^{-1} for GM_1 simply from the ratio of reverse and forward rate constants (*6*). We determined an apparent avidity of $\sim 5 \times 10^{-10}$ M^{-1} for FAM-CT to surfaces containing 0.5 mol % GM_1, a value similar to the one reported using radiolabeled CT and whole cells (*2*).

From the crystal structure, it was determined that the terminal galactose contributes 39% to the binding to CT while the adjacent *N*-acetylgalactosamine (galNAc) possesses only 17% of all contacts (*31*). Of the gangliosides tested, only GM_1, $GD1_b$, and asialo-GM_1 contain a terminal galactose as well as an adjacent galNAc residue, suggesting that this two-sugar finger is sufficient for recognition. The terminal sialic acid in GM_1, known as the thumb of the "two-finger−thumb grip", together with the terminal galactose are the major interaction sites between the receptor and CT. The sialic acid "thumb" is either extended by an additional sialic acid residue in $GD1_b$ or shortened by the removal of this residue in asialo-GM_1, suggesting that the proper length of the sialic acid thumb is required to stabilize the CT−ganglioside interaction.

CONCLUSION

In sum, the present study proposes a mechanistic description of the multivalent interaction of CTB with GM_1 that is based on quantification of kinetic rate constants and affinities. Our data reveal the importance of receptor density and mobility for receptor cross-linking in multivalent ligand−receptor interactions. We also report for the first time that the presence of the A-subunit results in binding to GM_1-containing supported bilayers that has significant higher affinity than the pentameric membrane-binding B-subunit alone. We find that CTB and CT bind with high avidity to GM_1 and that the low-affinity interactions with $GD1_b$ and asialo-GM_1 require high concentrations of these receptors for observation. Compared to binding of CTB, we also find a stronger interaction of the whole toxin with $GD1_b$ and asialo-GM_1 that consistently suggests a role for the A-subunit in the binding step. This study also demonstrates that flow cytometry provides a powerful quantitative tool for the in vitro analysis of interactions of membrane-associated molecules (by reconstructing the cell surface onto microspheres) that allows receptor−ligand and multivalency effects to be investigated.

ACKNOWLEDGMENT

We thank Dr. Larry Sklar for helpful discussions on aspects of ligand−receptor interactions and Mr. Robb C. Habbersett for customizing the IDLYK flow cytometry data analysis program to facilitate kinetic analysis. We also thank Ms. Yolanda Valdez for assistance with labeling of toxin.

REFERENCES

1. Keizer, J. (1985) *Acc. Chem. Res. 18*, 235−241.
2. Cuatrecasas, P. (1973) *Biochemistry 12*, 3547−3558.
3. Cuatrecasas, P. (1973) *Biochemistry 12*, 3558−3566.
4. Schön, A., and Freire, E. (1989) *Biochemistry 28*, 5019−5024.
5. Terrettaz, S., Stora, T., Duschl, C., and Vogel, H. (1993) *Langmuir 9*, 1361−1369.
6. Kuziemko, G. M., Stroh, M., and Stevens, R. C. (1996) *Biochemistry 35*, 6375−6384.
7. MacKenzie, C. R., Hirama, T., Lee, K. K., Altman, E., and Young, N. M. (1997) *J. Biol. Chem. 272*, 5533−5538.
8. Cooper, M. A., Hansson, A., Lofas, S., and Williams, D. H. (2000) *Anal. Biochem. 277*, 196−205.
9. Nolan, J. P., and Sklar, L. A. (1998) *Nat. Biotechnol. 16*, 633−638.
10. Nolan, J. P., Lauer, S., Prossnitz, E. R., and Sklar, L. A. (1999) *Drug Discovery Today 4*, 173−180.
11. Nolan, J. P., Shen, B. H., Park, M. S., and Sklar, L. A. (1996) *Biochemistry 35*, 11668−11676.
12. Shen, B. H., Nolan, J. P., Sklar, L. A., and Park, M. S. (1997) *Nucleic Acids Res. 25*, 3332−3338.
13. Efron, B., and Tibshirani, R. (1986) *Stat. Sci. 1*, 54−77.
14. Smoluchowski, M. V. (1917) *Z. Phys. Chem. 92*, 129−168.
15. Shoup, D., and Szabo, A. (1982) *Biophys. J. 40*, 33−39.
16. Goldstein, B., and Dembo, M. (1995) *Biophys. J. 68*, 1222−1230.
17. Hlavacek, W. S., Perelson, A. S., Sulzer, B., Bold, J., Paar, J., Gorman, W., and Posner, R. G. (1999) *Biophys. J. 76*, 2421−2431.
18. Hlavacek, W. S., Posner, R. G., and Perelson, A. S. (1999) *Biophys. J. 76*, 3031−3043.
19. Malmqvist, M. (1994) *J. Mol. Recognit. 7*, 1−7.
20. Hornick, C. L., and Karush, F. (1972) *Immunochemistry 9*, 325−340.
21. Crothers, D. M., and Metzger, H. (1972) *Immunochemistry 9*, 341−357.
22. Subramanian, K., Holowka, D., Baird, B., and Goldstein, B. (1996) *Biochemistry 35*, 5518−5527.
23. Erickson, J. P. R., Goldstein, B., Holowka, D., and Baird, B. (1991) in *Biophysical and Biochemical Aspects of Fluorescence Spectroscopy* (Dewey, T., Ed.) pp 169−195, Plenum Press, New York.
24. Goins, B., Masserini, M., Barisas, B. G., and Freire, E. (1986) *Biophys. J. 49*, 849−856.
25. Wolf, A. A., Jobling, M. G., Wimer-Mackin, S., Ferguson-Maltzman, M., Madara, J. L., Holmes, R. K., and Lencer, W. I. (1998) *J. Cell Biol. 141*, 917−927.
26. Orlandi, P. A., and Fishman P. H. (1998) *J. Cell Biol. 141*, 905−915.
27. Myszka, D. G., He, X., Dembo, M., Morton, T. A., and Goldstein, B. (1998) *Biophys. J. 75*, 583−594.
28. Zhang, R. G., Scott, D. L., Westbrook, M. L., Nance, S., Spangler, B. D., Shipley, G. G., and Westbrook, E. M. (1995) *J. Mol. Biol. 251*, 563−573.
29. Orlandi, P. A., and Fishman, P. H. (1993) *J. Biol. Chem. 268*, 17038−17044.
30. Jacob, C. O., Sela, M., Pines, M., Hurwitz, S., and Arnon, R. (1984) *Proc. Natl. Acad. Sci. U.S.A. 81*, 7893−7896.
31. Merritt, E. A., Sarfaty, S., Vandenakker, F., Lhoir, C., Martial, J. A., and Hol, W. G. J. (1994) *Protein Sci. 3*, 166−175.
32. Goldstein, B., and Wofsy, C. (1996) *Immunol. Today 17*, 77−80.

BI0112816